MULTIPHASE RANS SIMULATION OF TURBULENT BUBBLY FLOWS

M. Colombo, M. Fairweather
Institute of Particle Science and Engineering, School of Chemical and Process Engineering,
University of Leeds, Leeds LS2 9JT, United Kingdom
M.Colombo@leeds.ac.uk; M.Faiweather@leeds.ac.uk

S.Lo, A. Splawski
CD-adapco, Didcot, Oxfordshire, United Kingdom

ABSTRACT

The subject of this paper is the CFD simulation of adiabatic bubbly air-water flows. The aim is to contribute to the ongoing effort to develop more advanced simulation tools and, perhaps even more challenging, support the case for a more confident application of these techniques to reactor safety studies. The focus of this work is mostly multiphase turbulence and our ability to predict it, since it is a major driver in many areas of multiphase flow modelling, in addition to work on population balance approaches for bubble size prediction and boiling at a wall. The models are validated against a large number of pipe flows which were selected as test cases for both their relative simplicity with respect to the more complex flows encountered in practice, and also for the significant number of experimental studies available. Both upward and downward flows are simulated with the STAR-CCM+ code. Starting from an existing formulation, an optimized bubble induced turbulence model is proposed and compared with other models available from the literature. The model is then included in a Reynolds stress multiphase formulation, which is assessed against experiments and the *k*-*ε* model. In this context, the availability of a validated Reynolds stress multiphase formulation would be a significant step forward for the simulation of more complex flow conditions given the known shortcomings of eddy viscosity-based turbulence models. Finally, the performance of a drag model that accounts for the effect of bubble aspect ratio is evaluated because of its ability to improve velocity predictions near the wall.

KEYWORDS
Computational multiphase fluid dynamics; Eulerian two-fluid model; air-water bubbly flow; two-phase turbulence; Reynolds stress model

1. INTRODUCTION

Gas-liquid multiphase flows are found in a large variety of industrial applications, such as nuclear reactors, chemical and petrochemical processes, boilers and heat exchange devices amongst many others, and in a multitude of natural phenomena as well. The physics of these flows is complicated by the discontinuity of properties at the interface between the phases and hydrodynamics, as well as interphase exchanges of mass, momentum and energy, which all depend on the internal geometry of the phase distribution which might be in the form of different patterns (e.g. bubbly flow, slug flow, annular flow, mist flow). In view of these complications, which pose great challenges to our ability to predict these flows, it is not surprising that research is still ongoing within many engineering disciplines, and in thermal hydraulics in particular, despite them having been studied for decades.

In recent years, computational multiphase fluid dynamics (CMFD) has started to emerge as a promising tool for the analysis and prediction of multiphase flows. In the nuclear field in particular, CMFD promises to be able to solve thermal hydraulic and safety issues which have resisted full understanding and accurate prediction for some time [1]. For the latter to be achieved, effort must be put in to the development of advanced simulation tools and associated modelling improvements and, perhaps even more challenging, in to supporting the case for a more confident application of these techniques to reactor safety studies. Even recently, application of CMFD to engineering and real system scale calculations has been limited to averaged Eulerian-Eulerian formulations coupled with Reynolds averaged Navier-Stokes (RANS) turbulent flow modelling approaches [2]. In two-fluid Eulerian-Eulerian formulations, the phases are treated as interpenetrating continua, and the conservation equations for each phase are derived from an averaging procedure that allows both phases to co-exist at any point. Therefore, only a statistical description of the interphase properties is available, and interfacial mass, momentum and energy exchanges require explicit modelling with proper closure relations [2-4].

In this paper, air-water bubbly flows inside vertical pipes are simulated with a two-fluid Eulerian-Eulerian model. The main focus of the work is the simulation of multiphase turbulence and the bubble contribution to the continuous phase turbulence, since these are major drivers in many areas of multiphase flow modelling. Over the years, adiabatic bubbly flows have been investigated by numerous researchers and our ability to predict them has been significantly improved. Advances have been achieved in the description of the forces acting on bubbles [5, 6] and, by combining two-fluid CMFD models and population balance approaches [7], of interactions between bubbles and the continuous medium, and amongst bubbles themselves. Most of the modelling in these areas requires knowledge of the multiphase turbulence field [8, 9], which therefore demands careful attention if further progress is to be made. The presence of bubbles modifies the structure of the liquid turbulence field and the production of shear-induced turbulence [10, 11], which in turn modifies bubble distribution and the bubble break-up and coalescence processes as well. Bubbles also act as a source of bubble-induced turbulence, the net result of which might be the suppression or augmentation of turbulence depending on the particular flow conditions [6, 12].

During the period 1970-1980, many attempts were made to model turbulence in multiphase flows. The first works were based on ad-hoc phenomenological modifications to turbulence models for the liquid phase [13]. Later on, researches were focused on the rigorous derivation of turbulence equations for multiphase flow [14, 15]. Understanding that multiphase turbulence is far from a linear superposition of bubble-induced and single-phase flow turbulence, the latter authors included source terms due to the presence of a dispersed phase directly into the equations of the turbulence model. Kataoka and Sherizawa [16] derived a two-equation turbulence model for a gas-liquid, two-phase flow using ensemble averaging of local instantaneous equations. In their model, turbulence is generated by the bubbles mainly through the work done by interfacial forces.

Since that time, different forms of bubble-induced source terms have been proposed, but a generally accepted form is yet to emerge. In bubbly flows, the drag-source model, where all the energy lost by bubbles due to drag is converted to turbulence kinetic energy in their wakes, has been generally adopted. Troshko and Hassan [17] derived a two-equation turbulence model from [16] and assumed bubble-induced turbulence to be entirely due to the work of interfacial force density per unit time. Amongst the interfacial forces, only drag was considered in the model, this being generally dominant in bubbly flows. In the turbulence energy dissipation rate equation, the interfacial term is assumed proportional to the bubble-induced production multiplied by the frequency of bubble-induced turbulence destruction, calculated from the bubble length scale and residence time [18]. Politano et al. [19] developed a k-ε model for turbulent polydispersed two-phase flows, including a bubble-induced source due to drag. In the turbulence dissipation rate equation, these authors assumed the same timescale as for the single-phase turbulence. Yao and Morel [7] also considered the contribution to bubble-induced turbulence of virtual mass. Their timescale includes the bubble diameter and turbulence dissipation rate. Rzehak and Krepper [20] proposed a mixed time scale, calculated from the bubble length scale and the liquid phase turbulence velocity scale. After comparison with other models available in the literature, these authors suggested it as a starting point for an improved model of bubble-induced turbulence.

Compared to two-equation turbulence models, comparatively fewer efforts have been dedicated to the development of Reynolds stress models (RSM) for two-phase bubbly flows. RSM are based on the solution of transport equations for the Reynolds stresses and they are not constrained by the use of an eddy-viscosity. In their RSM, Lopez de Bertodano et al. [21] accounted for bubble-induced turbulence through drag and assumed the same timescale as the single-phase turbulence. Lahey and Drew [22] derived an algebraic RSM from the linear superposition of shear-induced and bubble-induced Reynolds stresses. Mimouni et al. [23] developed an RSM where the source term due to bubbles is included through a correlation between the pressure and velocity fluctuations at the interface. The single-phase turbulence timescale is again used. The higher accuracy of the RSM with respect to a k-ε formulation was demonstrated through comparison with bubbly flow experimental data in a 2×2 rod bundle.

This paper aims to be a contribution to CFD simulation of gas-liquid bubbly flows, with a particular interest in the prediction of multiphase turbulence inside these flows. Both bubble-induced turbulence modelling and, in view of its potential and the lesser attention received in the literature, the development of a Reynolds stress multiphase formulation for bubbly flows are the main focus. Air-water bubbly flows inside vertical pipes were selected as the test case since they provide relatively simple flow conditions and have been tested in numerous experimental works. To ensure model validation over an extended range of conditions, a database of a large number of different flows has been built. Some downflow conditions are also included, since they have received much less attention in the literature [17, 21]. In addition to multiphase turbulence, the database is also exploited to compare the accuracy of different drag models. Correlations including the effect on drag of bubble aspect ratio, similar to that of Tomiyama et al. [24], have been considered only recently in CMFD models [6]. In particular, higher bubble aspect ratios near a solid wall increase drag and reduce the relative velocity between the phases in the near-wall region [24]. In view of its ability to improve phase velocity predictions near the wall, the correlation of Tomiyama et al. [24] is compared with other drag models and validated against experiments.

Clearly, validation against relevant experiments is a fundamental step for the confident utilization of any CMFD methodology. Here, numerous experimental studies in vertical pipes available in the literature are exploited, in both upflow [6, 11, 12, 25-29] and downflow [12, 30, 31] conditions. At the beginning of the paper, the focus is on the modelling of bubble-induced turbulence. Starting from the formulation due to Rzehak and Krepper [20], validation is extended to a wider range of experiments and a further optimization of the model is proposed, which is then compared against the Rzehak and Krepper [20] model itself and the model from Troshko and Hassan [17]. The same bubble-induced turbulence model is then added to a multiphase Reynolds stress formulation. The RSM is validated against the same experimental database and methods of incorporating wall effects in the pressure-strain correlation, and their coupling with the two-phase flow field, are discussed. Later, the database is exploited to compare different drag models and their behaviour in the near-wall region in particular. Finally, validation of the CMFD model is extended to downward pipe flows.

2. EXPERIMENTAL DATA

To ensure validation of the models over an extended range of geometrical parameters and operating conditions, 19 flows were selected from 6 different sources. Experimental measurements are taken from the works of Serizawa et al. [25], Wang et al. [12], Liu and Bankoff [26], Liu [27], Kashinsky and Radin [31] and Hosokawa and Tomiyama [6]. Data includes air-water upward and downward flows in pipes, characterized by both wall-peaked and core-peaked void profiles. Data cover extended ranges of void fraction α (0.03-0.45), water superficial velocity j_w (0.5-1.4), air superficial velocity j_a (0.02-0.436) and hydraulic diameter D_h (0.025 m-0.06 m). Bubble diameters are generally within the range 3 mm to 4.25 mm, although some conditions giving significantly smaller bubbles are included for downward flows (0.8 mm and 1.5 mm). Details of the database are provided in Table I.

In Table I, when not directly available, averaged void fraction has been calculated from averaging of the radial void fraction profiles. Average inlet superficial velocities and void fraction provided in the papers noted were also compared with values calculated by integrating radial profiles. Discrepancies were found that required adjustment of the inlet values for some of the experiments [12, 25]. Also, the diameter of the bubbles was not available for all the experiments. For Wang et al. [12], values are provided in [17]. For Serizawa et al. [25], a value of d_B = 4 mm is given as an average for all the experiments. In Liu and Bankoff [26], a range between 2 mm and 4 mm is indicated by the authors. Given that more detailed information is not available, the mean value of d_B = 3 mm was used. Despite the large amount of experimental data available for two-phase flows in pipes, however, additional measurements extended to all the parameters of the flow, including bubble diameter and the continuous phase turbulence, are still necessary to improve our understanding and to allow improvements in numerical models.

Concerning turbulence measurements, only the r.m.s. of streamwise fluctuating velocity values are provided for most of the experiments. Although, measurements available show that an approximation of the wall-normal to streamwise r.m.s. of velocity fluctuations might be given by $v_w^2/u_w^2 \sim 0.5$, and, therefore, by $k \sim u_w^2$ for the turbulence kinetic energy [6, 12]. Therefore, values of streamwise fluctuating velocities from the experiments have been compared to $k^{0.5}$ from the k-ε simulations. This choice, also made in [20], aims to optimize the bubble-induced turbulence model to return the correct level of turbulence kinetic energy and to ensure a straightforward extension to a Reynolds stress formulation.

Table I Summary of the experimental conditions included in the validation database (*values calculated from radial profiles, $^+$values not given in original paper or averaged values).

Data	Source	j_w [m/s]	j_a [m/s]	α [-]	d_B [mm]	D_h [m]	Profile	Orientation
W1	Wang et al. [12]	0.71	0.1	0.100*	3.0^+	0.05715	Wall	Upflow
W2	Wang et al. [12]	0.94	0.4	0.202*	3.0^+	0.05715	Wall	Upflow
W3	Wang et al. [12]	0.43	0.4	0.383*	3.0^+	0.05715	Wall	Upflow
W4	Wang et al. [12]	0.668	0.082	0.152*	3.0^+	0.05715	Wall	Downflow
LB1	Liu and Bankoff [26]	0.753	0.180	0.143*	3.0^+	0.038	Wall	Upflow
LB2	Liu and Bankoff [26]	1.087	0.112	0.058*	3.0^+	0.038	Wall	Upflow
LB3	Liu and Bankoff [26]	0.376	0.347	0.456*	3.0^+	0.038	Core	Upflow
LB4	Liu and Bankoff [26]	1.391	0.347	0.210*	3.0^+	0.038	Wall	Upflow
L1	Liu [27]	0.5	0.12	0.152	2.94	0.0572	Wall	Upflow
L2	Liu [27]	1.0	0.22	0.157	3.89	0.0572	Wall	Upflow
S1	Serizawa et al. [25]	1.03	0.145	0.107	4.0^+	0.06	Wall	Upflow
S2	Serizawa et al. [25]	1.03	0.291	0.192	4.0^+	0.06	Wall	Upflow
S3	Serizawa et al. [25]	1.03	0.436	0.259	4.0^+	0.06	Core	Upflow
H1	Hosokawa and Tomiyama [6]	1.0	0.036	0.033	3.66	0.025	Wall	Upflow
H2	Hosokawa and Tomiyama [6]	0.5	0.025	0.04	4.25	0.025	Core	Upflow
K1	Kashinsky and Radin [31]	0.5	0.0194	0.0383	0.8	0.0423	Core	Downflow
K2	Kashinsky and Radin [31]	0.5	0.0924	0.162	0.8	0.0423	Core	Downflow
K3	Kashinsky and Radin [31]	1.0	0.0917	0.104	0.8	0.0423	Core	Downflow
K4	Kashinsky and Radin [31]	1.0	0.0917	0.108	1.5	0.0423	Core	Downflow

3. MATHEMATICAL MODEL

For the adiabatic air-water flows considered in this work, the two-fluid Eulerian-Eulerian model requires continuity and momentum equations for both phases, treated as incompressible:

$$\frac{\partial}{\partial t}(\alpha_k \rho_k) + \frac{\partial}{\partial x_i}(\alpha_k \rho_k U_{i,k}) = 0 \tag{1}$$

$$\frac{\partial}{\partial t}(\alpha_k \rho_k U_{i,k}) + \frac{\partial}{\partial x_j}(\alpha_k \rho_k U_{i,k} U_{j,k}) = -\alpha_k \frac{\partial}{\partial x_i} p_i + \frac{\partial}{\partial x_j}\left[\alpha_k\left(\tau_{ij,k} + \tau_{ij,k}^{Re}\right)\right] + \alpha_k \rho_k g_i + M_{i,k} \tag{2}$$

In the above equations, α_k represents the volume fraction of phase k, whereas in the following only α is used to represent the void fraction of air. $\boldsymbol{\tau}$ and $\boldsymbol{\tau}^{Re}$ are the laminar and turbulent stress tensors, respectively. The term M_k accounts for momentum exchanges between the phases due to interfacial forces. In this work, the drag force, lift force, wall force and turbulent dispersion force are included. The drag force is an expression of the resistance, opposed to bubble motion, by the surrounding liquid and numerous correlations for the drag coefficient have been proposed over the years. The Wang [32] correlation was derived for air-water bubbly flows at near atmospheric pressure, using curve-fitting of measurements of single bubbles rising in water. In Tomiyama et al. [24], a more theoretical formulation is proposed, where the effect of the bubble aspect ratio E on the drag coefficient is also accounted for:

$$C_D = \frac{8}{3} \frac{Eo}{E^{2/3}(1-E^2)^{-1} Eo + 16 E^{4/3}} F^{-2} \tag{3}$$

where F is a function of E and Eo is the bubble Eötvös number. Since knowledge of the aspect ratio is necessary in Eq. (3), a correlation is provided in [6]. Here, a slightly modified version is used, to avoid the asymptotic convergence to 0.65 of E_0 even for small spherical bubbles:

$$E = \max\left[1.0 - 0.35 \frac{y}{d_B}, E_0\right] \tag{4}$$

E_0 is calculated from Welleck et al. [33]. Concerning the lift force, a plethora of different models and correlations have been proposed for the lift coefficient. A thorough review is provided in [34]. Although the correlation of Tomiyama et al. [35] has been adopted by many authors [20], in our case it did not provide satisfactory agreement with experiments and a constant value $C_L = 0.1$ is preferred. It should be noted that a constant value has also been adopted by a number of authors, and good agreement with data has been reported in the literature using values ranging from 0.01 [12] to 0.5 [23]. A negative value of $C_L = -0.05$ was chosen to account for the lift coefficient change of sign in core-peaked profiles. A similar very weak lift coefficient for large bubbles is also reported in [17]. The wall force is modelled using the approach of Antal et al. [36], with optimized wall force coefficients $C_{w1} = -0.055$ and $C_{w2} = 0.09$. The turbulent dispersion force is modelled accordingly to Burns et al. [37].

Turbulence is resolved only in the continuous phase and it is modelled with a multiphase formulation of the standard k-ε turbulence model [38]:

$$\begin{aligned}\frac{\partial}{\partial t}\left((1-\alpha)\rho_c k_c\right) + \frac{\partial}{\partial x_i}\left((1-\alpha)\rho_c U_{i,c} k_c\right) \\ = \frac{\partial}{\partial x_j}\left[(1-\alpha)\left(\mu_c + \frac{\mu_{t,c}}{\sigma_k}\right)\frac{\partial}{\partial x_j} k_c\right] + (1-\alpha)\left(P_{k,c} - \rho_c \varepsilon_c\right) + (1-\alpha) S_k^{BI}\end{aligned} \tag{5}$$

$$\frac{\partial}{\partial t}\big((1-\alpha)\rho_c\varepsilon_c\big)+\frac{\partial}{\partial x_i}\Big((1-\alpha)\rho_c U_{i,c}\varepsilon_c\Big)$$
$$=\frac{\partial}{\partial x_j}\left[(1-\alpha)\left(\mu_c+\frac{\mu_{t,c}}{\sigma_\varepsilon}\right)\frac{\partial}{\partial x_j}\varepsilon_c\right]+(1-\alpha)\left[\frac{\varepsilon_c}{k_c}\big(C_{\varepsilon,1}P_{k,c}-C_{\varepsilon,2}\rho_c\varepsilon_c\big)+S_\varepsilon^{BI}\right] \tag{6}$$

P is the production of turbulence kinetic energy, $\mu_{t,c}$ is the turbulent viscosity and $C_{\varepsilon,1}$ = 1.44, $C_{\varepsilon,2}$ = 1.92, σ_k = 1.0 and σ_ε = 1.3. Turbulence in the dispersed phase is computed with a response coefficient, in view of the very low value of the density ratio in air-water flows. Turbulence in the dispersed phase is therefore assumed equal to turbulence in the continuous phase. Indeed, experimental measurements suggest that this equality is approached starting from void fractions as small as 6 % [39]. To account for the bubble contribution to turbulence, appropriate bubble-induced source terms are introduced in Eq. (7) and Eq. (8). The drag force $\boldsymbol{F_d}$ is considered as the only source of turbulence generation due to bubbles and all the energy lost by the bubbles to drag is assumed to be converted into turbulence kinetic energy inside the bubble wakes:

$$S_k^{BI}=K_{BI}\boldsymbol{F_d}\boldsymbol{U_r} \tag{7}$$

K_{BI} modulates the turbulence source. After comparison with the whole database, an optimum value K_{BI} = 0.25 was chosen that will be discussed in more detail in the results section. In the turbulence dissipation rate equation, the bubble-induced source term is expressed as the corresponding turbulence kinetic energy source term multiplied by the timescale of the bubble-induced turbulence τ_{BI}. Throsko and Hassan [17] assumed the bubble-induced timescale to be proportional to the bubble residence time ($\tau_{BI} \sim |\boldsymbol{U_r}| / d_B$). Following [20], in this work a mixed timescale is instead adopted, with a velocity scale derived from the liquid turbulence kinetic energy and a length scale equal to the bubble diameter:

$$S_\varepsilon^{BI}=\frac{C_{\varepsilon,BI}}{\tau_{BI}}S_k^{BI}=1.0\frac{k^{0.5}}{d_B}S_k^{BI} \tag{8}$$

In addition to the k-ε model, a multiphase Reynolds stress formulation is also used. The transport equations for the Reynolds stresses R_{ij}, based on the Gibson and Launder formulation [40], are [38]:

$$\frac{\partial}{\partial t}\Big((1-\alpha)\rho_c R_{ij}\Big)+\frac{\partial}{\partial x_j}\Big((1-\alpha)\rho_c U_{i,c}R_{ij}\Big)$$
$$=\frac{\partial}{\partial x_j}\big[(1-\alpha)D_{ij}\big]+(1-\alpha)\big(P_{ij}+\Phi_{ij}-\varepsilon_{ij}\big)+(1-\alpha)S_{ij}^{BI} \tag{9}$$

D_{ij} is the Reynolds stress diffusion and Φ_{ij} is the pressure-strain model, which accounts for pressure fluctuations that redistribute energy amongst the normal stresses. The pressure-strain model includes wall reflection terms, introduced to account for the presence of a solid wall that modifies the pressure field and blocks the transfer of energy from the streamwise to the wall normal direction. In this paper, other than the linearly decreasing model with wall distance [40], a quadratic function f_w which accounts for a faster decay of wall damping is also tested [41]:

$$f_w=\left(\frac{k^{3/2}}{\varepsilon}\frac{1}{C_l y_w}\right)^2 \tag{10}$$

where the constant $C_l = 2.5$. The bubble-induced source term is calculated using Eq. (7) or Eq. (8) and then split amongst the normal Reynolds stress components [21]. With respect to [21], the largest fraction of bubble-induced turbulence source is accommodated in the streamwise direction:

$$S_{ij}^{BI} = \begin{bmatrix} 1.0 & 0.0 & 0.0 \\ 0.0 & 0.5 & 0.0 \\ 0.0 & 0.0 & 0.5 \end{bmatrix} S_k^{BI} \tag{11}$$

4. RESULTS AND DISCUSSION

The system of equations and models noted above were solved using the STARCCM+ code [38]. All the simulations were made in a two-dimensional axisymmetric geometry, imposing inlet velocities, void fraction and outlet pressure as boundary conditions. At the inlet, flat profiles were imposed and the flow was allowed to evolve along the pipe to reach steady-state fully developed conditions. A strict convergence of residuals was ensured, together with a mass imbalance under 0.1 %. After a mesh sensitivity study on a limited number of conditions, it was found that an equidistant structured mesh with a first grid point close to $y^+ = 30$, which is a lower limit for the use of a wall function, was sufficient to ensure mesh independent solutions. Therefore, for the remaining cases the mesh was adjusted proportionally maintaining a first grid point as close as possible to $y^+ = 30$.

In a first stage, bubble-induced turbulence models were tested against experiments with the k-ε model and for all the upward flow conditions. Comparisons included radial profiles of liquid velocity, void fraction and the r.m.s. of velocity fluctuations. Figure 1 shows results for 4 of those cases. In general, good agreement was found with data for the liquid velocity and void fraction. However, more difficult to predict were core-peaked void profiles (Figure 1 j-l). Void fraction radial profiles in particular, which include a broader range of bubble diameters, with a majority of large deformed bubbles migrating towards the pipe centre but, still, also a significant number of smaller spherical bubbles remaining close to the wall, were difficult to reproduce using a constant bubble diameter. Further improvements in this regard might be reached by adding a population balance model to describe the whole bubble diameter spectrum. Better agreement is shown for wall-peaked void profiles. In particular, the flat profile of the liquid velocity and the void peak near the wall are well predicted in all conditions.

Comparison of streamwise r.m.s. velocities is shown for Troshko and Hassan [17], Rzehak and Krepper [20] and the optimized model in Eq. (7). The general overestimation obtained with [20] led to the addition of K_{BI} in Eq. (7), that was defined equal to 0.25 after comparison with experiments. A more complex dependancy on flow parameters was also investigated, but the evidence available is not conclusive so limiting K_{BI} to a constant value was retained for the present work. The uncertainity in bubble diameter for a significant number of experiments might have played a crucial role in this regard. Therefore, there is still the need for additional detailed experimental measurements for further improvements in these areas. As shown in Figure 1, Eq. (7) achieves satisfactory results in almost all conditions and improves predictions with respect to Rzehak and Krepper [20]. The worse results were found for the Liu and Bankoff [26] data (Figure 1 g-i), that were often underestimated. It could be argued here that the short distance between the inlet and the measurement plane in the experimental setup might have led to conditions that were not completely fully developed, and higher turbulence fluctuations with respect to other experiments. On average, a comparable level of accuracy was found for Troskho and Hassan [17]. However, results seem less consistent and show discrepancies from the experiments in some cases, as seen for case S1 in Figure 1d-f and H2 in Figure 1j-l. In addition, Eq. (7) allowed significant improvement in core-peaked profiles, where both Rzehak and Krepper [20] and Troskho and Hassan [17] overestimate the liquid turbulent fluctuations (Figure 1-l). Therefore, Eq. (7) can be considered as an improved formulation to account for the bubble-induced turbulence contribution in bubbly flows and it has been used in the simulations presented below.

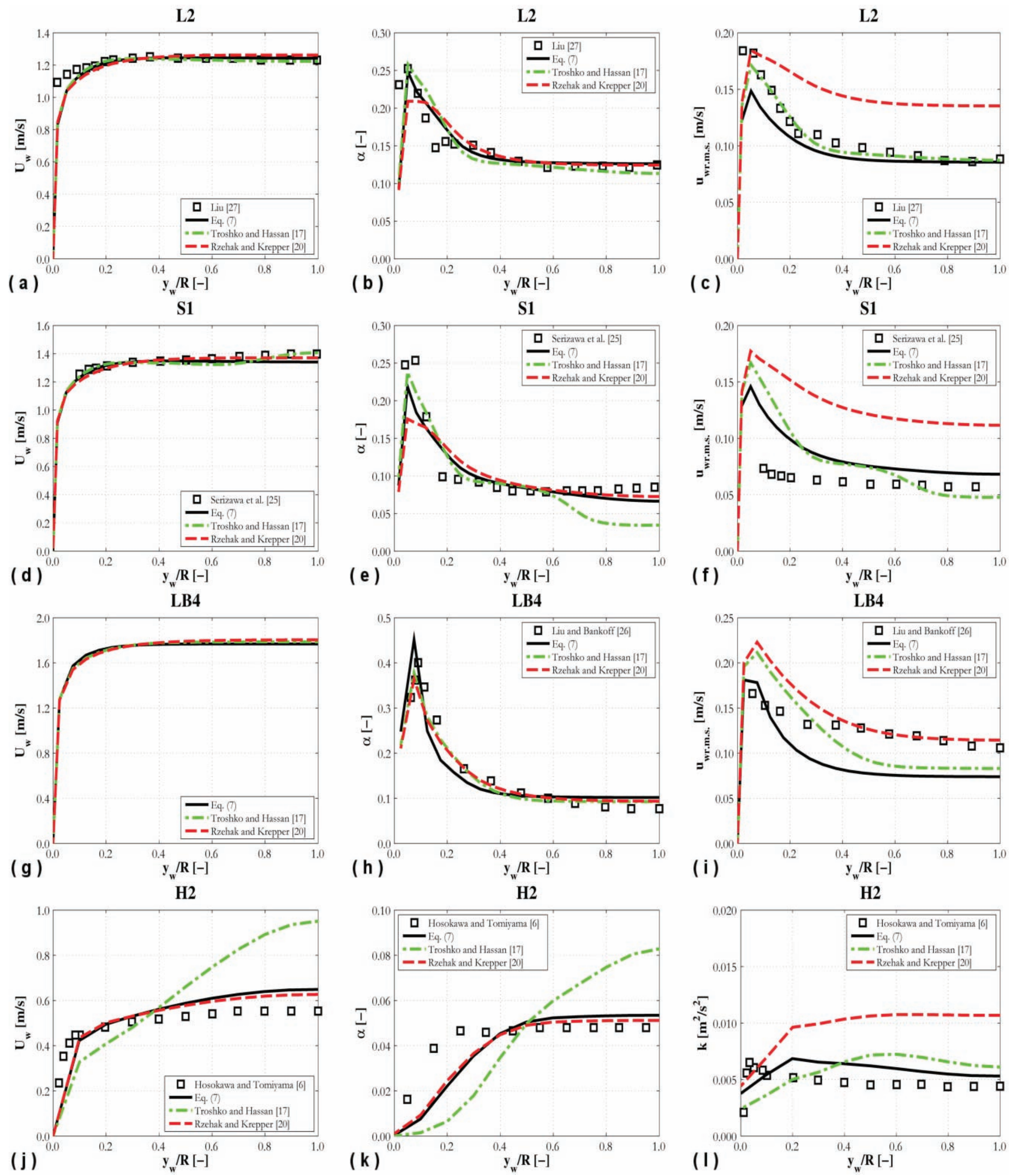

Figure 1 Comparison of radial profiles of calculated liquid velocity, void fraction and liquid r.m.s. streamwise fluctuating velocities against experiments for cases L2, S1, LB4 and H2. Bubble-induced turbulence models of Troshko and Hassan [17] (-.) and Rzehak and Krepper [20] (--) are compared with Eq. (7) (-).

Results for the Reynolds stress multiphase formulation obtained using Eq. (7) as the bubble-induced turbulence source are shown in Figure 2. First, attention is focused on experiment LB1 from [26], for which radial profiles of the r.m.s. radial velocity fluctuations are also available (Figure 2 a-c). For the Gibson and Launder [40] model, an increase of the void fraction in the pipe centre is visible (Figure 2-b), in addition to the peak at the wall. A similar increase is also shown by the liquid velocity (Figure 2-a), although no void fraction or liquid velocity increase in the pipe core region is visible for Naot and Rodi [41], the predictions of which are in agreement with experiments. The reason for this was identified in the shape of the radial $v_{w,\ r.m.s.}$ for Gibson and Launder [40], due to the interaction of the linearly decreasing wall reflection term, which was still significant near the centre of the pipe, with the flat turbulence profile generated by the presence of the bubbles. Actually, a flatter turbulence profile characterizes bubbly flows with respect to a single-phase flow, as can be noted from Figure 2-c and Figure 2-f, and also in Figure 1. From liquid momentum balances at steady-state, a gradient in the liquid radial Reynolds stress generates a radial pressure gradient with a lower pressure near the pipe axis. The momentum equation for the liquid remains balanced, but the same is not true for the air momentum balance, where the radial stress is almost negligible due to the low value of the air density. Therefore, the pressure gradient starts pushing the bubbles towards the axis, until it is balanced by the lift force caused by the velocity gradient induced by the increased void fraction. When wall reflection effects are instead limited to the near-wall region, the radial stress remains flat towards the pipe centre and predictions are in agreement with experiments.

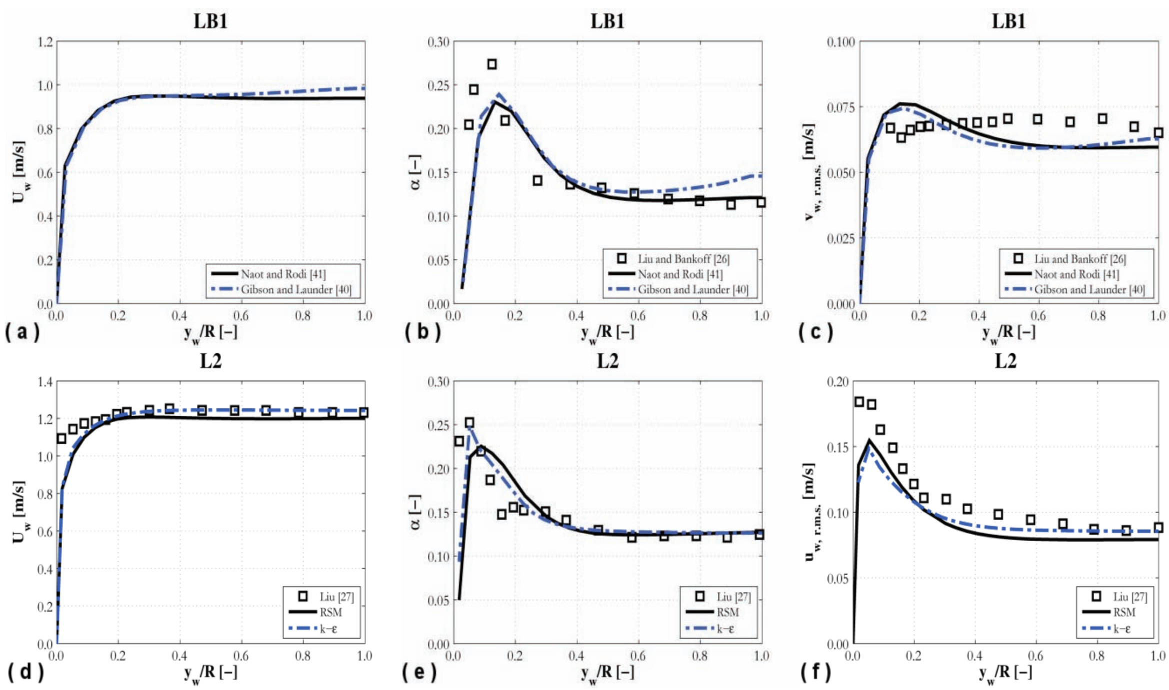

Figure 2 Comparison of radial profiles of calculated liquid velocity, void fraction and liquid r.m.s. radial fluctuating velocities against experiments for cases LB1 and L2. a-c include calculations from Gibson and Launder [40] and Naot and Rodi [41], whereas comparison between *k*-*ε* and RSM is shown in d-f.

RSM results including the Eq. (10) wall reflection damping and Eq. (7) for bubble-induced turbulence were comapred with *k*-*ε* predictions for a selected number of cases. Comparisons for experiment L2 are shown in Figure 2 d-f. Both models were found to be in satisfactory agreement with experiments. With respect to the flat velocity profile of the *k*-*ε* model, the RSM shows a slight peak near the wall followed by a dip towards the centre of the pipe, observed for all the tested conditions. This effect, which is not shown in the experiments, might be attributable to a higher sensitivity of the RSM to the drag by bubbles, moving at a higher velocity and with a higher concentration near the wall, on the liquid phase. The same effect was found for the *k*-*ε* model, but limited to experiment S2 only. In general, the RSM also predicts a slightly lower turbulence level in the pipe centre. Overall, results from the two models were found to be very similar and in satisfactory agreement with experiments.

Figure 3 shows results for the drag models of Wang [32] and Tomiyama et al. [24] coupled with [33] for the bubble aspect ratio. For experiment S2, results are particularly relevant, this being the only case where the dip in the liquid velocity profile towards the pipe centre was found for the *k-ε* model. The correlation of Tomiyama et al. [24] predicts a higher drag coefficient that causes a lower relative velocity in the centre of the pipe. More importantly, the drag coefficient is further increased near the wall by the higher aspect ratio, and a further reduction of the relative velocity is observed. As a consequence, agreement with experiments is improved, although the accuracy is instead worse in the pipe centre. Improvements near the wall generate a more general improvement of the liquid velocity profile, that does not show the dip towards the pipe centre anymore. Comparable results were obtained with the RSM (Figure 3-c). Radial velocity profiles are improved near the wall and do not show the dip in the pipe centre, which was found to affect particularly the RSM simulations. Instead, the relative velocity in the pipe centre is again underestimated.

Figure 3 e-h shows experiment H1 and RSM calculations. Also in this case, reduction of the relative velocity near the wall is more in agreement with experiments. In the pipe centre, Tomiyama et al. [24] again predicts a lower relative velocity. Unfortunately, no measurements are available at this location for this experiment. Differently from S2, liquid velocity profiles are very similar between the two drag models. The same is true for the r.m.s. of the velocity fluctuations (Figure 3-g), where the anisotropy is correctly predicted by the RSM. This, even if not relevant in these pipe flows, would help the prediction of other flows, such as in presence of turbulence-driven secondary flows in non-circular ducts. For the void fraction, changes in the relative velocity near the wall had a large impact on the magnitude of lift and wall forces, which essentially determine the void radial profile in these kinds of flow. Therefore, to maintain the same accuracy on void radial distribution (Figure 3-f), it was necessary to reoptimize the wall force coefficients to C_{w1} = -0.4 and C_{w2} = 0.3 for the *k-ε* model and C_{w1} = -0.65 and C_{w2} = 0.45 for the RSM. Summarizing, improvements in the near-wall region suggest using the Tomiyama et al. [24] correlation but, at the same time, worse predictions in the pipe centre suggest a need for further work.

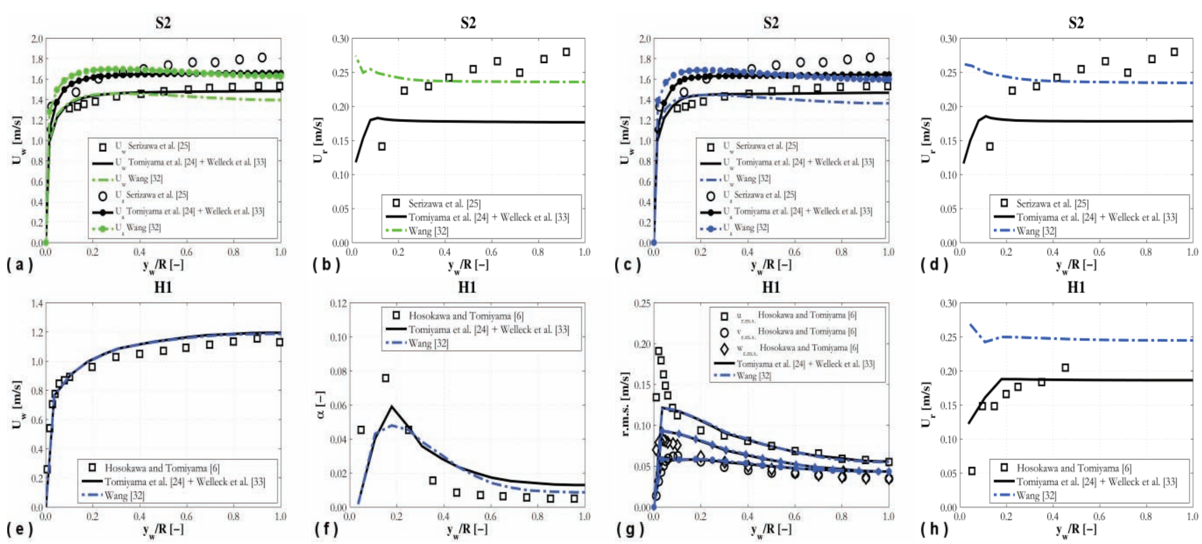

Figure 3 Comparison of drag models of Tomiyama et al. [24] and Wang [32] against experiments. a-d show liquid, air and relative velocity for *k-ε* and RSM against S2. e-h show liquid velocity, void fraction, liquid r.m.s. streamwise fluctuating velocities and relative velocity for RSM against H1. In Figure g: (no mark) $u_{r.m.s.}$; (●) $v_{r.m.s.}$; (♦) $w_{r.m.s.}$.

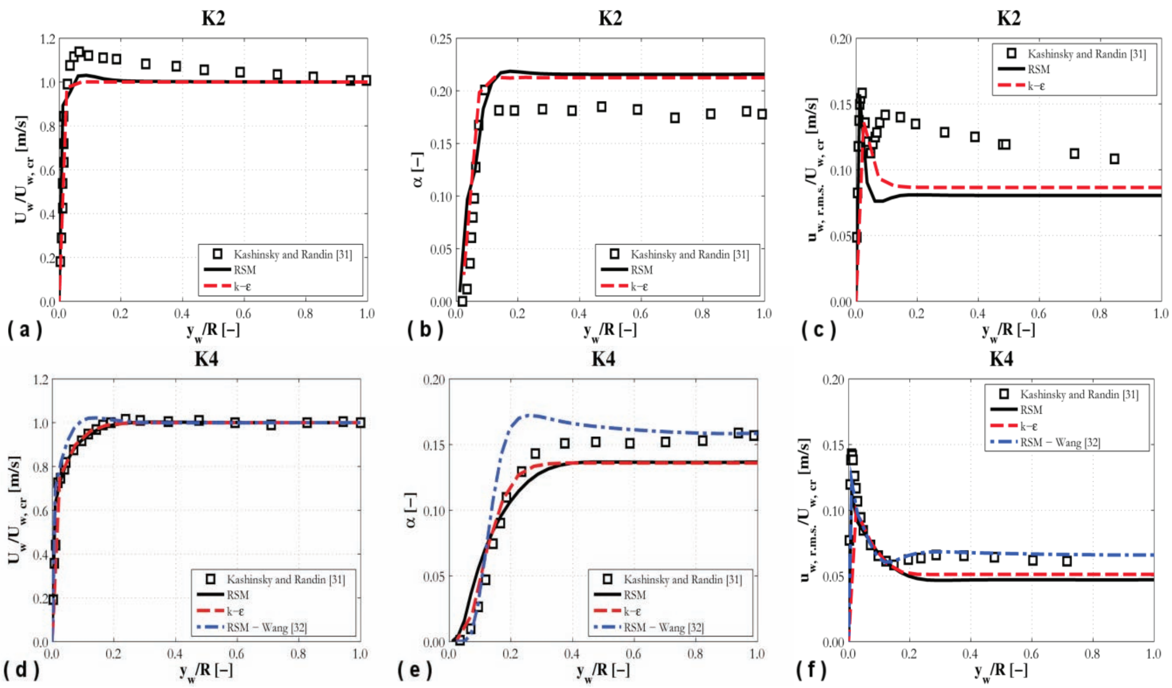

Figure 4 Comparison of radial profiles of calculated liquid velocity, void fraction and liquid r.m.s. streamwise fluctuating velocities against experiments for downward flows K2 and K4. a-c show calculations for *k-ε* and RSM for K2. d-f show calculations for k-ε (--), RSM (-) and RSM with Wang drag [32] (-.) for K4.

Finally, downward pipe flows have been considered for a further validation of both *k-ε* and RSM. In Figure 4, comparison is shown for experiments K2 and K4. Following the experiments, both the liquid velocity and water r.m.s. streamwise fluctuating velocities are normalized by the pipe centre velocity. Figure 4 helps to briefly highlight the general characteristics of bubbly downward flows. Lift force and wall force are both dirceted towards the centre, therefore a bubble free layer occupies the immediate vicinity of the wall, followed by an almost flat distribution towards the pipe centre. An almost flat velocity profile also characterizes downward flows, and a liquid velocity peak, generally known as the "chimney effect" [12], may sometimes be observed at the wall. Liquid velocity magnitude is higher than the air velocity magnitude, so that bubbles retard the flow in the pipe centre and higher liquid velocities may be found in the low void region near the wall.

Predictions of liquid velocity and void fraction profiles are in good agreement for both models, even if some discrepancies can be highlighted. In particular, the observed wall peak in the liquid velocity seems difficult to predict, as shown in Figure 4-a for experiment K2, where it is underestimated by both models. This peak is not, however, evident in K4 and the velocity profiles are in good agreement. Void fraction is well predicted in both cases, despite a slight overestimation at the lowest liquid superficial velocity in K2. For experiment K4, the drag model of Wang [32] is also compared. For the experiments at d_B = 0.8 mm, where bubbles are very close to a spherical shape, differences were negligible amongst the drag models. In contrast, the drag model of Tomiayama et al. [24] again predicts an underestimated relative velocity in the centre of the pipe, even if only an indirect indication of this can be found in the lower void fraction and turbulent velocity fluctuations shown in Figure 4-e and Figure 4-f

Similar behaviour of the water r.m.s. streamwise velocity fluctuations were predicted by the models, even when they are not in agreement with experiments. In particular, as shown in Figure 4-c and Figure 4-f, they are accurate for the K4 experiment (d_B = 1.5 mm), but are underestimated for K2 (d_B = 0.8 mm). This may be related to difficulties of the model in handling low bubble diameter conditions, where the length scale of the bubble is less comparable to the length scale of the turbulence. In these conditions, the conversion of drag work to turbulence kinetic energy in the bubble wakes might not be the dominant bubble-induced contribution, due to both the smaller length scale of the bubble and the lower relative velocity. In this regard, future efforts will be directed towards the development of a more advanced model, able to account for "pseudo-turbulence" generation due to liquid displacement by random bubble movements [10]. It is also worth mentioning here that smaller diameter bubbles increase the ability of turbulence to displace the bubbles after interaction with turbulent eddies.

5. CONCLUSIONS

Air-water bubbly flows were simulated in this work with a two-fluid Eulerian-Eulerian multiphase model and the STARCCM+ code. With the aim of improving currently available formulations, in particular in the field of multiphase turbulence modelling, an optimized model for bubble-induced turbulence has been proposed, starting from that developed by Rzehak and Krepper [20]. The model showed an improved accuracy with respect to other literature formulations over a wide range of flows, including both upward and downward flow conditions. Satisfactory accuracy was also obtained with a Reynolds stress turbulence model using the same bubble-induced turbulence model formulation. Although results were comparable to k-ε for pipe flows, RSM has the ability to overcome known drawbacks of two-equation, eddy viscosity-based turbulence formulations and is therefore of value in the simulation of more complex multiphase flows. Some drawbacks were also identified, the most important being a potential interaction between the two-phase field and the wall reflection formulation in the pressure-strain correlation. It is important to limit wall reflection effects to the near-wall region, where they are really effective, to avoid interaction with the two-phase field in the pipe centre that might generate unphysical behaviour not observable in a single-phase flow. Additional comparisons indicated that velocity predictions near the wall could be improved using a drag formulation that accounts for the increase in bubble aspect ratio and drag coefficient in the wall region.

Some potential future developments were also identified. A constant coefficient was used to modulate the bubble-induced turbulence source. Inclusion of more complex dependencies, such as the bubble length scale to turbulence length scale ratio, would be useful, even if it requires the availability of additional detailed experimental measurements. In addition, underestimation of the turbulence level at low bubble diameter (d_B = 0.8 mm) suggests the need for more complex turbulence models, where generation of turbulence by bubble random motion (which might be dominant at these diameters) is also accounted for. In the RSM, even if a faster decay of the wall effects in the pressure strain significantly improved the results, the adoption of more recently developed and advanced Reynolds stress formulations is strongly suggested and will be pursued in the future. Finally, a further improved drag model that maintains the benefits underlined in this work in the near-wall region, but does not at the same time worsen the results in the pipe centre, will also be pursued.

NOMENCLATURE

C_D	drag coefficient [-]	p	pressure [Pa]
$C_{\varepsilon,1}$, $C_{\varepsilon,2}$	model constants [-]	R	radius [m]
D_h	hydraulic diameter [m]	R_{ij}	Reynolds stress $\tau_{i,j}^{Re} / \rho_c$ [m^2 s^{-2}]
d_B	bubble diameter [m]	t	time [s]
E	bubble aspect ratio [-]	U	velocity [m s^{-1}]
Eo	bubble Eotvos number ($\Delta\rho g d_B^2/\sigma$) [-]	u, v, w	r.m.s. of velocity fluctuations [m s^{-1}]
F_D	drag force per unit volume [kg m^{-2} s^{-2}]	y_w	wall distance [m]
j	superficial velocity [m s^{-1}]	α	void fraction [-]
k	turbulence kinetic energy [m^2 s^{-2}]	ε	dissipation rate of k [m^2 s^{-3}]

μ	viscosity [Pa s]	σ	surface tension [N m^{-1}]
ρ	density [kg m^{-3}]	σ_k, σ_ε	model constants [-]

Subscripts

a	air	*r*	relative
BI	bubble-induced	*t*	turbulent
c	continuous phase	*w*	water

ACKNOWLEDGEMENTS

The authors gratefully acknowledge the financial support of the EPSRC under grant EP/K007777/1, Thermal Hydraulics for Boiling and Passive Systems, part of the UK-India Civil Nuclear Collaboration.

REFERENCES

1. G. Yadigaroglu, “CMFD and the critical-heat-flux grand challenge in nuclear thermal-hydraulics – A letter to the editor of this special issue”, *Int. J. Multiphase Flow* **67**, pp. 3-12 (2014).
2. A. Prosperetti and G. Tryggvason, *Computational methods for multiphase flow*, Cambridge University Press, Cambridge, United Kingdom (2009).
3. D.A. Drew, “Mathematical modeling of two-phase flow”, *Annu. Rev. Fluid Mech.* **15**, pp. 261-291 (1983).
4. M. Ishii and T. Hibiki, *Thermo-fluid dynamics of two-phase flow*, Springer, USA (2006).
5. D. Lucas, E. Krepper and H.M. Prasser, “Use of models for lift, wall and turbulent dispersion forces acting on bubbles for poly-disperse flows”, *Chem. Eng. Sci.* ***62***, pp. 4146-4157 (2007).
6. S. Hosokawa and A. Tomiyama, “Multi-fluid simulation of turbulent bubbly pipe flow”, *Chem. Eng. Sci.* **64**, pp. 5308-5318 (2009).
7. W. Yao and C. Morel, “Volumetric interfacial area prediction in upward bubbly two-phase flow”, *Int. J. Heat Mass Tran.* **47**, pp. 307-328 (2004).
8. Y. Liao and D. Lucas, “A literature review of theoretical models for drop and bubble breakup in turbulent dispersion. on mechanisms and models for the coalescence process of fluid particles”, *Chem. Eng. Sci.* **64**, pp. 3389-3406 (2009).
9. Y. Liao and D. Lucas, “A literature review on mechanisms and models for the coalescence process of fluid particles”, *Chem. Eng. Sci.* **65**, pp. 2851-2864 (2010).
10. M. Lance and J. Bataille, “Turbulence in the liquid phase of a uniform bubbly air-water flow”, *J. Fluid Mech.* **222**, pp. 95-118 (1991).
11. M.E. Shawkat, C.Y. Ching and M. Shoukri, “On the liquid turbulence energy spectra in two-phase bubbly flow in a large diameter pipe”, *Int. J. Multiphase Flow* **33**, pp. 300-316 (2007).
12. S.K. Wang, S.J. Lee, O.C. Jones Jr and R.T. Lahey Jr, “3-D turbulence structure and phase distribution measurements in bubbly two-phase flows”, *Int. J. Multiphase Flow* **13**, pp. 327-343 (1987).
13. Y. Sato, M. Sadatomi and K. Sekoguchi, “Momentum and heat transfer in two-phase bubbly flow-I. Theory”, *Int. J. Multiphase Flow* **7**, pp. 167-177 (1981).
14. S.E. Elghobashi and T.W. Abou-Arab, “A two-equation turbulence moodel for two-phase flows”, *Phys. Fluids* **26**, pp. 931-938 (1983).
15. D.C. Besnard and F.H. Harlow, “Turbulence in multiphase flow”, *Int. J. Multiphase Flow* **14**, pp. 679-699 (1989).
16. I. Kataoka and A. Serizawa, “Basic equations of turbulence in gas-liquid two-phase flow”, *Int. J. Multiphase Flow* **15**, pp. 843-855 (1989).
17. A.A. Troshko and Y.A. Hassan, “A two-equation turbulence model of turbulent bubbly flows”, *Int. J. Multiphase Flow* **27**, pp. 1965-2000 (2001).

18. M. Lopez de Bertodano, R.T. Lahey Jr and O.C. Jones, "Development of a k-ε model for bubbly two-phase flow", *J. Fluids Eng.* **116**, pp. 128-134 (1994).
19. M.S. Politano, P.M. Carrica and J. Converti, "A model for turbulent polydisperse two-phase flow in vertical channels", *Int. J. Multiphase Flow* **29**, 1153-1182 (2003).
20. R. Rzehak and E. Krepper, "CFD modeling of bubble-induced turbulence", *Int. J. Multiphase Flow* **55**, 138-155 (2013).
21. M. Lopez de Bertodano, S.J. Lee, R.T. Lahey Jr and D.A. Drew, "The prediction of two-phase turbulence and phase distribution phenomena using a Reynolds stress model", *J. Fluids Eng.* **112**, pp. 107-113 (1990).
22. R.T. Lahey Jr and D.A. Drew, "The analysis of two-phase flow and heat transfer using a multidimensional, four field, two-fluid model", *Nucl. Eng. Des.* **204**, pp. 29-44 (2001).
23. S. Mimouni, J. Lavieville, N. Seiler and P. Ruyer, "Combined evaluation of second order turbulence model and polydispersion model for two-phase boiling flow and application to fuel assembly analysis", *Nucl. Eng. Des.* **241**, pp. 4523-4536 (2011).
24. A. Tomiyama, G.P. Celata, S. Hosokawa and S. Yoshida, "Terminal velocity of single bubbles in surface tension dominant regime", *Int. J. Multiphase Flow* **28**, pp. 1497-1519 (2002).
25. A. Serizawa, I. Kataoka, I. Michiyoshi, "Turbulence structure of air-water bubbly flow-II. Local properties", *Int. J. Multiphase Flow* **2**, pp. 235-246 (1975).
26. T.J. Liu and S.G. Bankoff, "Structure of air-water bubbly flow in a vertical pipe-I. Liquid mean velocity and turbulence measurements", *Int. J. Heat Mass Tran.* **36**, pp. 1049-1060 (1993).
27. T.J. Liu, "The role of bubble size on liquid phase on liquid phase turbulent structure in two-phase bubbly flows", *Proceedings of the 3rd International Conference on Multiphase Flow*, Lyon, France (1998)
28. T. Hibiki, M. Ishii and Z. Xiao, "Axial interfacial area transport of vertical bubbly flows", *Int. J. Heat Mass Tran.* **44**, pp. 1869-1888 (2001).
29. S. So, H. Morikita, S. Takagi and Y. Matsumoto, "Laser Doppler velocimetry measurement of turbulent bubbly channel flow", *Exp. Fluids* **33**, pp. 135-142 (2003).
30. V.E. Nakoryakov, O.N. Kashinsky, V.V. Randin and L.S. Timkin, "Gas-liquid bubbly flow in vertical pipes", *J. Fluids Eng.* **118**, pp. 377-382 (1996).
31. O.N. Kashinsky and V.V. Randin, "Downward bubbly gas-liquid flow in a vertical pipe", *Int. J. Multiphase Flow* **25**, pp. 109-138 (1999).
32. D.M. Wang, "Modelling of bubble flow in a sudden pipe expansion", *Technical Report II-34*, BRITE/EuRam Project BE-4098 (1994).
33. R.M. Welleck, A.K. Agrawal and A.H.P. Skelland, "Shape of liquid drops moving in liquid media" *AIChE J.* **12**, pp. 854-862 (1966).
34. T. Hibiki and M. Ishii, "Lift force in bubbly flow systems", *Chem. Eng. Sci.* **62**, pp. 6457-6474 (2007).
35. A. Tomiyama, H. Tamai, I. Zun and S. Hosokawa, "Transverse migration of single bubbles in simple shear flows", *Chem. Eng. Sci.* **57**, pp. 1849-1858 (2002).
36. S.P. Antal, R.T. Lahey Jr and J.E. Flaherty, "Analysis of phase distribution in fully developed laminar bubbly two-phase flow", *Int. J. Multiphase Flow* **17**, pp. 635-652 (1991).
37. A.D. Burns, T. Frank, I. Hamill and J.M. Shi, "The Favre averaged drag model for turbulent dispersion in Eulerian multi-phase flows", *5th International Conference on Multiphase Flow*, Yokohama, Japan, May 30 – June 4 (2004).
38. CD-adapco, *STAR-CCM+® Version 9.06 User Guide* (2014).
39. A. Behzadi, R.I. Issa and H. Rusche, "Modelling of dispersed bubble and droplet flow at high phase fractions", *Chem. Eng. Sci.* **59**, pp. 759-770 (2004).
40. M.M. Gibson and B.E. Launder, "Ground effects on pressure fluctuations in the atmospheric boundary layer", *J. Fluid Mech.* **86**, pp. 491-511 (1978).
41. D. Naot and W. Rodi, "Numerical simulation of secondary currents in channel flow", *J. Hyd. Eng. Div.-ASCE* **108**, pp. 948-968 (1982).